Evolution of Intermolecular Structure and Dynamics in Supercritical Carbon Dioxide with Pressure: An ab Initio Molecular Dynamics Study

Moumita Saharay† and Sundaram Balasubramanian*

Chemistry and Physics of Materials Unit, Jawaharlal Nehru Centre for Advanced Scientific Research, Jakkur, Bangalore 560 064, India

Received: September 1, 2006; In Final Form: October 28, 2006

The effect of pressure on supercritical carbon dioxide ($scCO_2$) has been characterized by using Car−Parrinello molecular dynamics simulations. Structural and dynamical properties along an isotherm of 318.15 K and at pressures ranging from 190 to 5000 bar have been obtained. Intermolecular pair correlation functions and three-dimensional atomic probability density map calculations indicate that the local environment of a central CO_2 molecule becomes more structured with increasing pressure. The closest neighbors are predominantly oriented in a distorted T-shaped geometry while neighbors separated by larger distances are likely oriented in a slipped parallel arrangement. The structure of $scCO_2$ at high densities has been compared with that of crystalline CO_2. The probability distributions of intramolecular distances narrow down with increasing pressure. A marginal but non-negligible effect of pressure on the instantaneous intramolecular OCO angle is observed, lending credence to the idea that intermolecular interactions between CO_2 molecules in an inhomogeneous near neighbor environment could contribute to the observed instantaneous molecular dipole moment. The extent of deviation from a perfect linear geometry of the carbon dioxide molecule decreases with increasing pressure. Time constants derived from reorientational time correlation functions of the molecular backbone compare well with experimental data. Within the range of thermodynamic conditions explored here, no significant changes are observed in the frequencies of intramolecular vibrational modes. However, a blue shift is observed in the low-frequency cage rattling mode with increasing pressure.

1. Introduction

The unique properties of supercritical CO_2 ($scCO_2$) with liquid-like densities and gas-like transport[1] make it an environmentally benign solvent[2−5] for various solutes.[6−8] The critical temperature and pressure of CO_2 are 304.2 K and 73.8 bar, respectively. The density of the supercritical fluid can even be doubled by doubling the pressure,[9] a feature that is characteristic of compressible fluids and unlike that of normal liquids. The solubility of solid solutes in $scCO_2$ has been shown to increase with increasing pressure of the solvent.[10] Despite being such a facile experimental tool that is employed to tune the properties of the fluid, the effect of pressure on the molecular and intermolecular structure and dynamics in this system remains not well studied. Motivated by this aim, we report here results of ab initio molecular dynamics simulations of $scCO_2$ based on the Car−Parrinello (CPMD) approach.[11] This method has been applied to study a wide variety of liquids and processes therein.[12]

Neutron diffraction measurements on high-pressure supercritical CO_2[13,14] show that the intermolecular structure factors depend primarily on the density of the solvent and are insensitive to temperature, in the ranges studied. It is reported that the T-shaped near neighbor configuration[15] around a solvent molecule becomes more structured at higher pressures due to electric multipole interactions. Our earlier works[16,17] on pristine CO_2 (318.15 K and 130 bar) showed that oxygen atoms of CO_2 molecules surround a central molecule in a plane perpendicular to its backbone. Similar near neighbor arrangements have also been reported by other classical MD simulations.[18−20] The near neighbor structure in $scCO_2$ is highly sensitive to its density. In the gas phase, the "slipped parallel" geometry between two neighboring CO_2 molecules is energetically more favorable than the T-shaped geometry.[21,22] The preference appears to be reversed in the liquid.[23] It was also speculated that CO_2 molecules could adopt nonlinear geometries in their instantaneous configurations due to polarization by neighboring molecules in the coordination shell.[17] Thus, although under isolated conditions in its electronic ground state carbon dioxide is a nondipolar molecule, an induced dipole moment could arise through interactions with near neighbors.

Here, we aim to obtain a microscopic picture of the changes in the intermolecular structure and dynamics of $scCO_2$ that are brought upon by an increase in the pressure. The work can also enable us to distinguish between the contributions from thermal factors and induced polarization due to near neighbors on the deviation from a linear geometry in the instantaneous configurations of carbon dioxide. In pursuit of these aims, we report here results obtained from extensive ab initio molecular dynamics simulations carried out at four different densities along an isotherm at 318.15 K. Anticipating our results, we find a marginal, but systematic effect of density on the intramolecular structure, while the intermolecular structure shows significant changes with increasing pressure. Data on the rotational dynamics of CO_2 molecules are also provided. We present the details of simulation in the next section followed by a description of the results.

2. Simulation Details

CPMD simulations[24] have been carried out along an isotherm at 318.15 K and at densities of 0.80444, 1.1, 1.216, and 1.4

* Address correspondence to this author. E-mail: bala@jncasr.ac.in.
† E-mail:moumita@jncasr.ac.in.

10.1021/jp065679t CCC: $37.00
Published on Web 12/15/2006

g/cm^3. These densities correspond to experimentally observed pressures of 190, 1034, 2000, and 5025 bar, respectively.[25] Each simulated system contained 32 CO_2 molecules. The simulations were performed in cubic supercells in the NVT ensemble. To obtain a reliable estimate of pressure in ab initio MD simulations, one is required to employ larger values of the plane wave energy cutoff than what is used here. Our simulations are carried out under constant density conditions, and the pressure values referenced in the discussion are obtained from experiments.[25] Three-dimensional periodic boundary conditions were applied. The box lengths at these densities were 14.27, 12.86, 12.43, and 11.86 Å, respectively. Our earlier work[26] had shown that the near-neighbor structure is unchanged for systems consisting of either 32 or 64 molecules. Hence a smaller system size was employed here.

The CPMD simulations at each state point were started from configurations which were equilibrated by classical MD simulations employing the EPM2[27] potential model. The equilibration runs in these classical MD simulations were of 100 ps duration each. At the start of each CPMD run, the electronic wavefunctions were quenched to the Born−Oppenheimer surface. CPMD calculations were carried out within the density functional approximation. The exchange and correlation functionals were from the works of Becke[28] and Lee, Yang, and Parr,[29] respectively. The electronic orbitals of valence electrons were expanded in a plane wave basis set with an energy cutoff of 70 Ry for the orbitals. Norm-conserving pseudopotentials of the Troullier−Martins form[30] were employed for the treatment of the core electrons. CPMD simulations with similar procedures as described here, but of reactive forms of carbon dioxide at much higher temperatures and pressures, have been carried out recently.[31] The fictitious mass of electrons was set to 500 au and the equations of motion were integrated with a time step of 4 au (around 0.096 fs). Temperature control for the ions was achieved by the use of a Nosé−Hoover chain thermostat.[32] The fictitious electronic kinetic energy was seen to be conserved throughout the molecular dynamics trajectory without the use of an electronic thermostat. To achieve better ensemble averaged properties of the solvent, the analysis run lengths at 1.216 and 1.4 g/cm^3 were higher than that at lower densities. Leaving a short span of 2 ps for equilibration at all the densities, the results at 0.80444, 1.1, 1.216, and 1.4 g/cm^3 were analyzed over 13, 13, 18.6, and 21.3 ps, respectively. The value of the mean squared displacement of CO_2 molecules in the densest system was found to be 55 Å^2 at 7 ps. Hence, we are satisfied that the molecules are labile and that the structural data reported here are well averaged.

3. Results and Discussion

3.1. Structure. *3.1.1. Pair Correlation Function.* The intermolecular structure of pure carbon dioxide in the supercritical state has been studied by neutron diffraction measurements[13,23] at densities ranging from 11 to 15 molecules/nm^3 over a wide variety of temperatures. Our work reported here consists of systems at densities varying between 11 and 19 molecules/nm^3. Hence a comparison between our ab initio results and the neutron data is possible. The partial radial distribution function, $g_{CC}(r)$, shown in Figure 1 exhibits a monotonic shift in the position of the first peak toward lower distances with increase in pressure. In addition, the peak becomes narrower indicating a better definition of the first coordination shell.

Significant changes in the solvent structure can be observed, however, in the intermolecular $g_{CO}(r)$, which is shown in Figure 2. The first peak at the lowest density is present at 4.2 Å and it shifts to shorter distances with increasing density, as expected. Interestingly, a hump develops in the first peak at moderate pressures and transforms into a distinct prepeak at the highest density studied, at 1.4 g/cm^3. This feature is present at around 3.1 Å. These observations are found to be consistent with the radial distribution functions obtained from neutron scattering measurements.[23] To investigate the origin of this new feature at 3.1 Å, we have examined the crystal structure of α-CO_2, in its Pa-3 form.[33,34] In a unit cell of the crystal, CO_2 molecules occupy the face centered cubic sites and the orientations of the molecular backbone axes are parallel to the body diagonals.

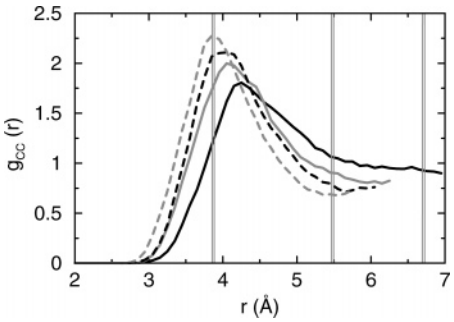

Figure 1. Intermolecular partial radial distribution functions between C−C pairs of CO_2 molecules at densities of 0.80444 (solid black), 1.1 (thick solid gray), 1.216 (dashed black), and 1.4 (dashed gray) g/cm^3 under supercritical conditions at 318.15 K. The thin gray vertical lines are the same function for crystalline CO_2. The latter are not completely shown along the *y*-axis.

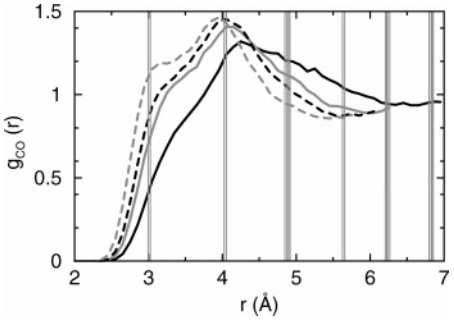

Figure 2. Intermolecular partial radial distribution functions between C−O pairs of CO_2 molecules, with the same description as in Figure 1.

Shown in the same figure are the pair correlation functions obtained from the crystal. One can observe the presence of a strong peak at 3.0 Å for the crystal, which is quite close to the prepeak observed in $scCO_2$ at 1.4 g/cm^3. It is worthy to point out here that the density of the crystal is 1.76 g/cm^3. Despite the difference in the density between $scCO_2$ at 1.4 g/cm^3 studied in our simulations and that of the crystal, the distance from the nearest oxygen to a central carbon is approximately the same. This comparison is further validated by an examination of the second peak in the $g_{CO}(r)$, which is present at 3.9 and 4.05 Å in the high-density fluid and the crystalline phases, respectively. Figure 3 shows the running coordination numbers of intermolecular oxygen atoms around a carbon in $scCO_2$ at 1.4 g/cm^3 and in the crystal. The curve for the former closely follows the data for the crystal, indicating that near-neighbor spatial correlations in $scCO_2$ at the highest density studied here possess features which are comparable to that in the crystal.

3.1.2. Atomic Probability Density Map. To identify the location of the near-neighbor oxygen atom around a central CO_2 molecule in $scCO_2$, we have calculated the three-dimensional atomic probability density map. Shown in Figure 4a are these data for the system at 1.4 g/cm^3, where isosurfaces in two shades

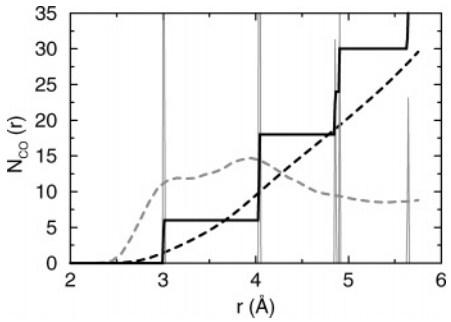

Figure 3. Comparison between running coordination numbers, $N_{CO}(r)$, of oxygen atoms surrounding a central carbon atom in the crystal (solid black) and in the supercritical fluid at 1.4 g/cm^3 (dashed black). The corresponding pair correlation functions are also shown in solid gray and dashed gray lines, respectively. The $g_{CO}(r)$ for the supercritical fluid has been multiplied by a factor of 10, and that for the crystal is incompletely shown.

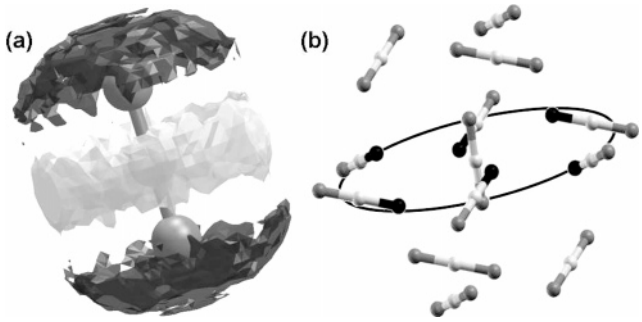

Figure 4. (a) Probability density map for the occurrence of neighboring oxygen atoms around a central CO_2 molecule with two different conditions on the intermolecular C−O separation, r_{CO}: (i) $r_{CO} < 3.4$ Å (gray isosurface) and (ii) $3.6 < r_{CO} < 4.3$ Å (black isosurface). The isosurface value for both surfaces is 0.07 oxygen atoms/Å^3, which is about twice the mean density of oxygen atoms in the system. (b) First coordination shell of CO_2 molecules in the crystal, where the C−C distance is 3.9 Å. The six closest oxygen atoms which are located near the equatorial plane are shown as black spheres. The ellipse is a caricature of this plane. Carbon atoms are shown in white and oxygen atoms are in gray.

are seen. The isosurface values for both are the same, 0.07 atoms/Å^3, which is about twice the mean density of oxygen atoms in this system. The surface in gray exhibits the location of oxygen atoms of neighboring CO_2 molecules which fall within a distance of 3.4 Å from a central carbon atom, while that in black is for oxygens present at distances between 3.6 and 4.3 Å. We can thus infer that the oxygen atoms which contribute to the new prepeak at 3.1 Å in the $g_{CO}(r)$ are mostly located on the equatorial plane around a central carbon dioxide molecule, while those which contribute to the primary first peak present at 3.9 Å are predominantly located in the polar regions around a central CO_2. This interpretation is further aided by a comparison of the near-neighbor structure in crystalline carbon dioxide. Shown in Figure 4b is the configuration of the closest 12 neighbors, i.e., the first coordination shell (based on intermolecular C−C distance) around a central CO_2 in the crystal. Around a molecule that is aligned along the *z*-axis, six molecules lie in or near the equatorial plane.

Six oxygen atoms from this group, one from each molecule, form the first oxygen coordination shell around the carbon of a central molecule, at a distance of 3.02 Å. Six other molecules are present near the poles of the central molecule. Their oxygen atoms form the second oxygen shell, at a distance of 4.05 Å. The parallels between the crystal structure analyzed in this fashion and the intermolecular structure in the fluid at the density

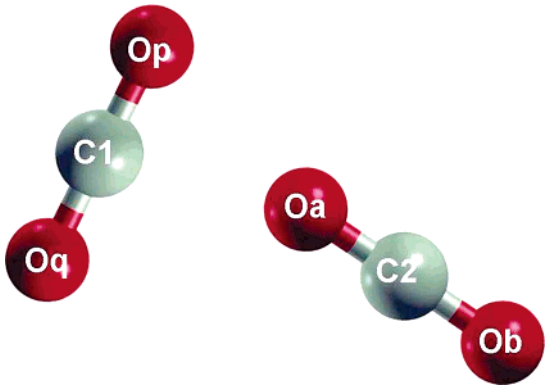

Figure 5. Schematic depicting a typical near-neighbor arrangement, which also defines the nomenclature used in the discussion. C_1 is the carbon of the central molecule and O_a is the intermolecular oxygen atom closest to it.

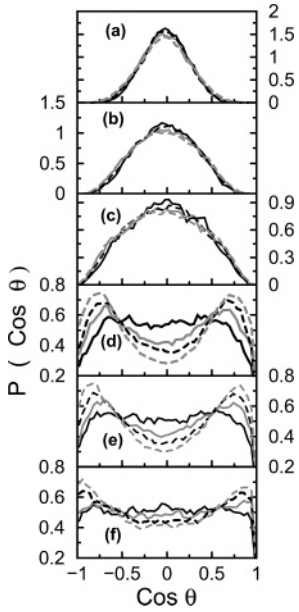

Figure 6. Probability distributions of $\widehat{O_pO_q}\cdot\widehat{O_1O_a}$ (a and d), $\widehat{O_pO_q}\cdot\widehat{O_1O_2}$ (b and e), and $\widehat{O_pO_q}\cdot\widehat{O_1O_b}$ (c and f) with C_1O_a cutoff (i) within 3.4 Å (a, b, c) and (ii) between 3.6 and 4.3 Å (d, e, f). The distributions correspond to the following density values: 0.80444 (solid black line), 1.1 (solid gray line), 1.216 (dashed black line), and 1.4 g/cm^3 (dashed gray line).

of 1.4 g/cm^3 are striking and lend further credence to our interpretation of the intermolecular structure in $scCO_2$ at high densities.

We shall now examine the orientational order of near-neighbor molecules and its evolution with density. To proceed further, we illustrate a typical near-neighbor configuration in Figure 5. C_1 is the central carbon atom bonded to O_p and O_q. The intermolecular oxygen atom closest to a carbon is denoted as O_a and the farther one is denoted as O_b. We are interested in finding out the orientation of near-neighbor pairs of molecules in $scCO_2$. The analysis has been divided into two parts, based on the C_1-O_a distance: (i) within the first prepeak of $g_{CO}(r)$, i.e., within 3.4 Å, and (ii) between 3.6 and 4.3 Å. Figure 6 exhibits the probability distributions of angles between the unit vector, $O_p\widehat{O_q}$, and various intermolecular vectors at all the densities. The distributions in Figure 6a−c exhibit a preference for cosθ values around zero for a distance cutoff of 3.4 Å, indicating that the closest neighboring molecules prefer a T-shaped or to be more precise a distorted T-shaped configu-

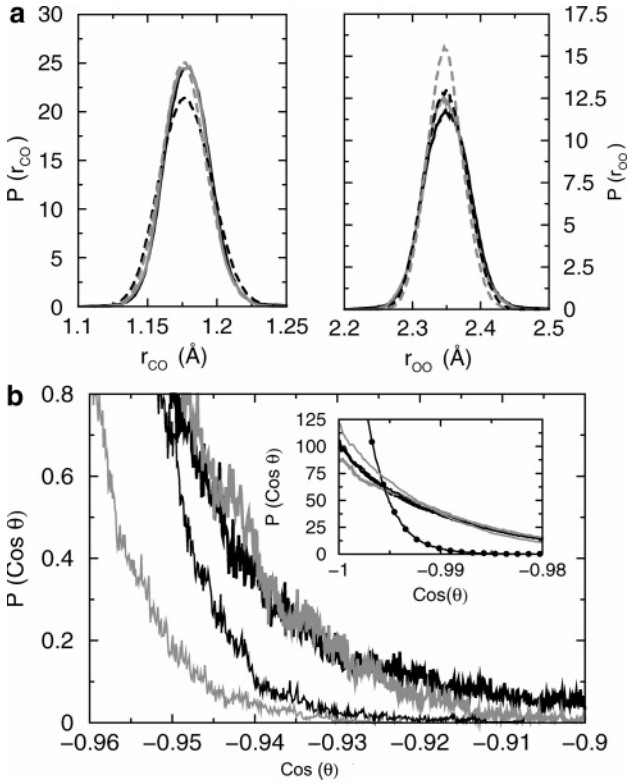

Figure 7. (a) Probability distributions of the intramolecular C−O (r_{CO}) and O−O (r_{OO}) distances. The distributions correspond to the following density values: 0.80444 (solid black line), 1.1 (solid gray line), 1.216 (dashed black line), and 1.4 g/cm^3 (dashed gray line). (b) Probability distributions of the intramolecular OCO angle, θ, of CO_2 molecules at the following densities: 0.80444 (thick black), 1.1 (thick gray), 1.216 (thin black), and 1.4 g/cm^3 (thin gray). The corresponding classical MD result with a harmonic bending potential for the system at a density of 1.4 g/cm^3 is shown in black circles. The inset shows the full distributions, and the main body highlights the tail regions.

ration. This feature in the near-neighbor arrangement is present irrespective of the system density and only a marginal effect of pressure on these distributions is observed. On the other hand, $P(\cos\theta)$ plots for C_1-O_a distances between 3.6 and 4.3 Å show a pronounced effect of pressure on intermolecular orientation. At the lowest density, 0.80444 g/cm^3, the distribution is almost isotropic in nature, whereas two distinct peaks at around 140° and 40° appear at higher densities. Thus, a pair of CO_2 molecules separated by distances between 3.6 and 4.3 Å favor the "slipped parallel" configuration at high pressures.

3.1.3. CO_2 Geometry. Having studied the intermolecular ordering as a function of pressure, we now examine the intramolecular geometry of CO_2 with increasing pressure. We have learned that increasing pressure decreases intermolecular distances. In Figure 7a, we show the probability distributions of intramolecular O−C and O−O distances in $scCO_2$. Although the distributions narrow down with increasing pressure, the mean values of O−C and O−O distances decrease only negligibly, by about 0.002 to 0.003 Å. Shown in Figure 7b are the intramolecular angle distributions calculated at different densities. The pressure dependence of the tail region of the O−C−O angle distribution clearly shows that increasing density tends to make the molecules closer to linear.

The angle distributions obtained from the CPMD simulations are compared with those obtained from classical MD simulations which employed rigid bond lengths and a harmonic potential governing the O−C−O angle (k_θ = 1236 kJ/mol/rad^2). The distribution of instantaneous angles obtained from the classical

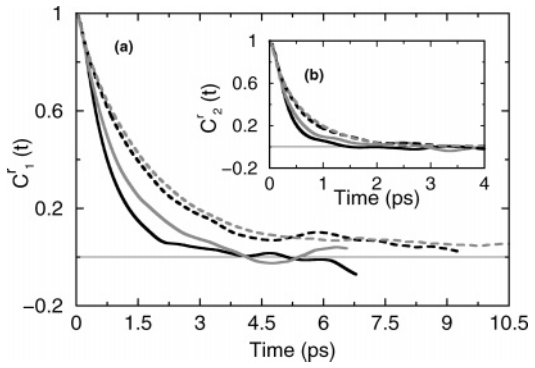

Figure 8. Reorientational time correlation functions of CO_2 backbone at the following values of density: 0.80444 (solid black line), 1.1 (solid gray line), 1.216 (dashed black line), and 1.4 g/cm^3 (dashed gray line). (a) First-order time correlation function (C_1^r) and (b) Second-order time correlation function (C_2^r).

simulations exhibits a much higher propensity for a linear geometry than the one from CPMD. This contrasting behavior between the classical and CPMD simulations and the pressure dependence observed in the CPMD angle distributions can be rationalized as due to polarization effects induced by a changing near-neighbor environment.

We believe that the deviation from linearity in the instantaneous geometry of CO_2 could have two underlying causes: (i) thermal fluctuations and (ii) the geometric distribution of near neighbors on or close to the equatorial plane around a central CO_2 molecule. Thermal effects are identical for all four systems studied as the simulations have been conducted at the same temperature, 318.15 K. Hence any differences in the intramolecular angle distributions between the systems, however marginal, must be ascribed purely to an increase in density. Inhomogeneities of molecular density in the instantaneous near-neighbor environment are likely to polarize a central CO_2, causing it to deviate away from a linear geometry. This is more likely to happen at lower densities than at higher densities. At lower densities in the supercritical state, a molecule is likely to be surrounded by fewer neighbors, leading to an anisotropic environment that in turn can polarize a central CO_2. At higher densities, the polarization effects from neighbors are likely to cancel each other, due to a progressively increasing homogeneous neighborhood. Our results on the intramolecular distance and angle distributions can thus be rationalized. Needless to say, in the crystalline PA-3 structure, the molecules are linear. Thus the trend toward an instantaneous linear geometry with increasing pressure in the supercritical state observed here is reasonable.

3.2. Dynamics. *3.2.1. Rotational Relaxation.* Increasing solvent density can have a marked effect on solvent dynamics. A crucial quantity to study in this regard is the rotational relaxation of carbon dioxide molecules, which can be investigated through NMR experiments.[35,36] In particular, these experiments probe the ^{17}O quadruple relaxation time of carbon dioxide, from which the reorientational relaxation time can be derived. Figure 8 depicts the calculated orientational correlation functions for CO_2 at different solvent densities. Consistent with earlier observations,[37,38] the rotational correlation functions are found to be quadratic in nature at low time scales at all densities. The orientational correlation function is defined as,

$$C_l^r(t) = \langle P_l(\mathbf{u}(0)\cdot\mathbf{u}(t))\rangle \qquad (1)$$

where **u** represents the unit backbone vector of CO_2 and l represents the order of Legendre polynomial. The integral

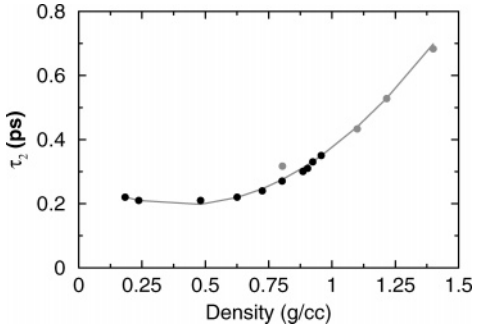

Figure 9. Comparison of the relaxation times τ_2^r between experiment (dark circles)[36] and that obtained from our simulations (gray circles), as a function of density of $scCO_2$.

correlation time can be calculated as,

$$\tau_l^r = \int_0^\infty C_l^r(t)\, dt \qquad (2)$$

The C_1^r correlation functions at 0.80444, and 1.1 g/cm^3 decay to zero within 4 ps. τ_1^r at these densities is 0.816 and 1.06 ps, respectively, while the same at 0.7 g/cm^3 had earlier been calculated to be 0.62 ps.[16] At higher densities, $C_1^r(t)$ decays much slower. τ_2^r has been calculated by integrating $C_2^r(t)$ (Figure 8b). We compare τ_2^r obtained from our simulations with experiment[36] in Figure 9. One finds a remarkably good agreement between experiment and our ab initio simulations. Although the experimental data at 319 K are available only up to a density around 0.957 g/cm^3, our simulation results appear to match well with its extrapolation. For densities higher than 0.8 g/cm^3, the rotational relaxation time increases steeply with increase in CO_2 density.

3.2.2. Vibrational Density of States. The density dependence of infrared[39,40] and Raman[41] spectra of supercritical carbon dioxide has been studied extensively by several experiments. We report here the vibrational density of states that depict both intra- and intermolecular modes in $scCO_2$. The power spectrum at each density has been obtained as a Fourier transform of the velocity auto time correlation function of the atoms. The resolution in wavenumber is around 5 cm^{-1} at 0.80444 and 1.1 g/cm^3 and around 3 cm^{-1} at 1.216 and 1.4 g/cm^3. In the range of pressures examined here at 318.15 K, no significant effect of pressure was observed on the frequencies of the fundamental modes of CO_2. Figure 10 shows the vibrational density of states of CO_2 at different state points. We do not observe any noticeable change in the peak positions of bending (υ_2) (Figure 10b), symmetric stretching (υ_1) (Figure 10c), and asymmetric stretching (υ_3) (Figure 10d) modes except for a relative contraction of the bandwidth with increase in system pressure. These bands have been discussed in detail in our earlier work.[16]

Crucial changes in the vibrational spectra of $scCO_2$ with pressure are observed in the external or intermolecular modes. Figure 10a shows the power spectra in the far-infrared region, between 0 and 200 cm^{-1}. With increasing density, we observe the emergence of a mode whose frequency shifts from around 15 cm^{-1} at 1.1 g/cm^3 to 50 cm^{-1} at 1.4 g/cm^3. The blue shift is discernible with increasing pressure. This mode is likely due to the rattling of molecules within cages formed by their neighbors. Cardini et al.[42] had observed this broad mode in liquid-like clusters of CO_2 modeled using an empirical potential. Our results agree quantitatively with the frequency range in which they observed this mode. The nonzero value of the power spectrum at zero frequency is due to molecular diffusion. Note

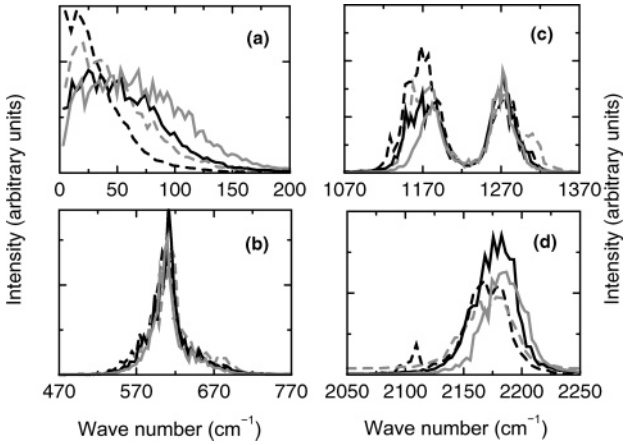

Figure 10. Vibrational density of states of supercritical CO_2 obtained from the Fourier transformation of velocity autocorrelation functions of all the atoms at the following densities: 0.80444 (dashed black line), 1.1 (dashed gray line), 1.216 (solid black line), and 1.4 (solid gray line) g/cm^3. (a) Cage rattling, (b) bending, (c) symmetric stretching, and (d) asymmetric stretching mode.

the decrease in its magnitude with increasing density, as expected.

4. Discussion and Conclusions

We have presented the results of ab initio molecular dynamics simulations of supercritical CO_2 performed under high pressures at $T = 318.15$ K. As stated in the section on simulation details, the pressures reported here are experimental data[25] which correspond to the state conditions of our simulations. The main aim of this work was to elucidate the effect of pressure on the structural and dynamical properties of this solvent. Analysis of the local environment of a CO_2 molecule shows (i) the progressive reorganization of the first coordination shell with increasing pressure and (ii) that the distorted T-shaped arrangement of the closest neighbors around a central molecule changes gradually to a "slipped parallel" like arrangement at farther distances. The distribution of the instantaneous O−C−O intramolecular angle shows a marginal preference toward linear geometry with increasing pressure. At higher densities, an increase in the coordination number can cause the polarization of a central molecule to cancel out, which may explain this observation. In an interesting report, Ladanyi and Parson[43] had studied the polarization of iodide ions embedded in a CO_2 cluster. They observed a strong polarization of the solute when the bending force constant of CO_2 was reduced, i.e., in a hyperflexible model. Our ab initio results on the pressure dependence of the induced polarization in CO_2 molecules is thus relevant. The emergence of a prepeak in the $g_{CO}(r)$ at a distance of around 3.1 Å at high densities is an important finding from our study. We have rationalized its presence by a detailed comparison with the intermolecular structure in crystalline CO_2. This comparison also enabled us to understand the orientational preference exhibited by intermolecular oxygen atom neighbors.

As regards the dynamics of the system, rotational relaxation times have been calculated from our simulations and an excellent agreement with experiment has been observed. As expected, the relaxation time τ_2^r derived from the second-order reorientational correlation function increases with pressure. The vibrational density of states calculated from the simulations demonstrates negligible changes in the peak frequency of intramolecular modes. Interestingly, a blue shift in the low-frequency intermolecular mode, which occurs due to cage rattling, is observed, consistent with earlier MD calculations

on CO_2 clusters.[42] At the highest density studied here, i.e., 1.4 g/cm^3, this mode is observed at 52 cm^{-1}.

The current work offers microscopic details on the intra- and intermolecular structure and dynamics of $scCO_2$ with pressure. It would now be interesting to study the pressure dependence of solvent organization around solutes.[44] This issue and its relevance to the calculation of chemical reaction rates in this solvent are likely to be topics of our future investigations.

Acknowledgment. The research reported here was supported in part by grants from the Council of Scientific and Industrial Research (CSIR) and the Department of Science and Technology, India. We acknowledge the Centre for Modelling, Simulation and Design, University of Hyderabad where some of the calculations were carried out.

References and Notes

(1) Shah, P. S.; Hanrath, T.; Johnston, K. P.; Korgel, B. A. *J. Phys. Chem. B* **2004**, *108*, 9574−9587.
(2) Leitner, W. *Nature* **2000**, *405*, 129−130.
(3) Poliakoff, M.; King, P. *Nature* **2001**, *412*, 125.
(4) Wells, S. L.; DeSimone, J. M. *Angew. Chem., Int. Ed.* **2001**, *40*, 518− 527.
(5) DeSimone, J. M. *Science* **2002**, *297*, 799−803.
(6) DeSimone, J. M.; Guan, Z.; Elsbernd, C. S. *Science* **1992**, *257*, 945−947.
(7) Li, Q.; Zhang, Z.; Zhong, C.; Liu, Y.; Zhou, Q. *Fluid Phase Equil.* **2003**, *207*, 183−192.
(8) Ribeiro, M. A.; Bernardo-Gil, M. G. *J. Chem. Eng. Data* **1995**, *40*, 1188− 1192.
(9) Clifford, T. *Fundamentals of Supercritical Fluids*; Oxford University Press: Oxford, UK, 1999.
(10) Hourri, A.; St-Arnaud, J. M.; Bose, T. K. *Rev. Sci. Instrum.* **1998**, *69*, 2732− 2737.
(11) Car, R.; Parrinello, M. *Phys. Rev. Lett.* **1985**, *55*, 2471−2474.
(12) Tuckerman, M. E. *J. Phys. Condens. Matter* **2002**, *14*, R1297−R1355.
(13) Chiappini, S.; Nardone, M.; Ricci, F. P.; Bellissent-Funel, M. C. *Mol. Phys.* **1996**, *89*, 975−987.
(14) Cipriani, P.; Nardone, M.; Ricci, F. P. *Phys. B* **1998**, *241*−*243*, 940−946.
(15) Ishii, R.; Okazaki, S.; Okada, I.; Furusaka, M.; Watanabe, N.; Misawa, M.; Fukunaga, T. *J. Chem. Phys.* **1996**, *105*, 7011−7021.
(16) Saharay, M.; Balasubramanian, S. *J. Chem. Phys.* **2004**, *120*, 9694−9702.
(17) Saharay, M.; Balasubramanian, S. *ChemPhysChem* **2004**, *5*, 1442−1445 Erratum: Saharay, M.; Balasubramanian, S. *ChemPhysChem* **2006**, *7*, 1167.
(18) Fedchenia, I. I.; Schröder, J. *J. Chem. Phys.* **1997**, *106*, 7749−7755.
(19) Zhang, Y.; Yang, J.; Yu, Y. X. *J. Phys. Chem. B* **2005**, *109*, 13375−13382.
(20) Zhang, Z.; Duan, Z. *J. Chem. Phys.* **2005**, *122*, 214507.
(21) Knozinger, E.; Beichert, P. *J. Phys. Chem.* **1995**, *99*, 4906−4911.
(22) Raveendran, P.; Wallen, S. *J. Am. Chem. Soc.* **2002**, *124*, 12590−12599.
(23) Cipriani, P.; Nardone, M.; Ricci, F. P.; Ricci, M. A. *Mol. Phys.* **2001**, *99*, 301−308.
(24) Hutter, J.; Ballone, P.; Bernasconi, M.; Focher, P.; Fois, E.; Goedecker, S.; Marx, D.; Parrinello, M.; Tuckerman, M. E. *CPMD*, Version 3.9.1; Max Planck Institut fuer Festkoerperforschung: Stuttgart; and IBM Zurich Research Laboratory: Zurich, 1997−2001.
(25) Thermophysical properties of fluid systems: http://webbook.nist.gov/chemistry/fluid.
(26) Saharay, M.; Balasubramanian, S. *J. Phys. Chem. B* **2006**, *110*, 3782−3790.
(27) Harris, J. G.; Yung, K. H. *J. Phys. Chem.* **1995**, *99*, 12021−12024.
(28) Becke, A. D. *Phys. Rev. A* **1988**, *38*, 3098−3100.
(29) Lee, C.; Yang, W.; Parr, R. G. *Phys. Rev. B* **1988**, *37*, 785−789.
(30) Troullier, N.; Martins, J. L. *Phys. Rev. B* **1991**, *43*, 1993−2006.
(31) Tassone, F.; Chiarotti, G. L.; Rousseau, R.; Scandolo, S.; Tosatti, E. *ChemPhysChem* **2005**, *6*, 1752−1756.
(32) Martyna, G. J.; Klein, M. L.; Tuckerman, M. *J. Chem. Phys.* **1992**, *97*, 2635−2643.
(33) Suzuki, M.; Schnepp, O. *J. Chem. Phys.* **1971**, *55*, 5349−5356.
(34) Olinger, B. *J. Chem. Phys.* **1982**, *77*, 6255−6258.
(35) Umecky, T.; Kanakubo, M.; Ikushima, Y. *J. Phys. Chem. B* **2003**, *107*, 12003−12008.
(36) Holz, M.; Haselmeier, R.; Dyson, A. J.; Huber, H. *Phys. Chem. Chem. Phys.* **2000**, *2*, 1717−1720.
(37) Haghighi, A. S.; Adams, J. E. *J. Phys. Chem. A* **2001**, *105*, 2680−2686.
(38) Adams, J. E.; Haghighi, A. S. *J. Phys. Chem. B* **2002**, *106*, 7973−7980.
(39) Yagi, Y.; Tsugane, H.; Inomata, H.; Saito, S. *J. Super. Crit. Fluids* **1993**, *6*, 139−142.
(40) Yokoyama, C.; Kanno, Y.; Takahashi, M.; Ohtake, K.; Takahashi, S. *Rev. Sci. Instrum.* **1993**, *64*, 1369−1370.
(41) Poliakoff, M.; Howdle, S. M.; Kazarian, S. G. *Angew. Chem., Int. Ed. Engl.* **1995**, *34*, 1275−1295.
(42) Cardini, G.; Schettino, V.; Klein, M. L. *J. Chem. Phys.* **1989**, *90*, 4441−4449.
(43) Ladanyi, B. M.; Parson, R. *J. Chem. Phys* **1997**, *107*, 9326−9338.
(44) Kanakubo, M.; Aizawa, T.; Kawakami, T.; Sato, O.; Ikushima, Y.; Hatakeda, K.; Saito, N. *J. Phys. Chem. B* **2000**, *104*, 2749−2758.